Robustness, efficiency, and optimality in the Fenna-Matthews-Olson photosynthetic pigment-protein complex

Lewis A. Baker and Scott Habershon[a)]
Department of Chemistry and Centre for Scientific Computing, University of Warwick, Coventry CV4 7AL, United Kingdom

(Received 9 April 2015; accepted 21 August 2015; published online 9 September 2015)

Pigment-protein complexes (PPCs) play a central role in facilitating excitation energy transfer (EET) from light-harvesting antenna complexes to reaction centres in photosynthetic systems; understanding molecular organisation in these biological networks is key to developing better artificial light-harvesting systems. In this article, we combine quantum-mechanical simulations and a network-based picture of transport to investigate how chromophore organization and protein environment in PPCs impacts on EET efficiency and robustness. In a prototypical PPC model, the Fenna-Matthews-Olson (FMO) complex, we consider the impact on EET efficiency of both disrupting the chromophore network and changing the influence of (local and global) environmental dephasing. Surprisingly, we find a large degree of resilience to changes in both chromophore network and protein environmental dephasing, the extent of which is greater than previously observed; for example, FMO maintains EET when 50% of the constituent chromophores are removed, or when environmental dephasing fluctuations vary over two orders-of-magnitude relative to the *in vivo* system. We also highlight the fact that the influence of local dephasing can be strongly dependent on the characteristics of the EET network and the initial excitation; for example, initial excitations resulting in rapid coherent decay are generally insensitive to the environment, whereas the incoherent population decay observed following excitation at weakly coupled chromophores demonstrates a more pronounced dependence on dephasing rate as a result of the greater possibility of local exciton trapping. Finally, we show that the FMO electronic Hamiltonian is not particularly optimised for EET; instead, it is just one of many possible chromophore organisations which demonstrate a good level of EET transport efficiency following excitation at different chromophores. Overall, these robustness and efficiency characteristics are attributed to the highly connected nature of the chromophore network and the presence of multiple EET pathways, features which might easily be built into artificial photosynthetic systems. © *2015 AIP Publishing LLC.* [http://dx.doi.org/10.1063/1.4930110]

I. INTRODUCTION

Photosynthesis underpins life on Earth, converting sunlight into the stored chemical energy which ultimately drives almost all biological processes. All photosynthetic systems operate by first absorbing sunlight in order to generate excited electronic states, and subsequently shuttling this excitation energy to a reaction centre (RC) where it can be used to drive the charge separation reactions which form the first steps in chemical energy storage.[1–3] To facilitate excitation energy transfer (EET) from the light-harvesting antenna complex to the RC, photosynthetic systems employ pigment-protein complexes (PPCs) which have evolved to provide high efficiency of light-to-charge conversion whilst allowing EET to proceed rapidly enough to avoid competitive excited-state quenching pathways.[1]

Much of the contemporary experimental and theoretical interest in photosynthetic PPCs has focussed on the role of quantum coherence in the mechanism and efficiency of EET.[1,3–12] Time-resolved non-linear spectroscopic studies suggest the existence of long-lived quantum "beats" in the population dynamics of PPCs demonstrating that quantum-mechanical effects may play a role in EET,[1,7,9,10,13] contrary to the textbook idea that such coherence should be "washed-out" by the thermal environment. In contrast, far less emphasis has been placed on answering a more fundamental question: why are PPCs built the way they are? Given the evolutionary time scales and the pressures of natural selection,[14,15] it is tempting to ask whether PPCs are specifically optimised for their role in the photosynthetic process or whether factors external to the EET process, such as synthetic accessibility or robustness to thermal fluctuations, are instead responsible for ultimately shaping the molecular organisation of PPCs. Answering such questions would, in turn, lead to a better understanding of how to construct improved artificial photosynthetic systems for water splitting,[16,17] or more efficient light-harvesting materials for solar energy technologies.[3,18] It is this question of optimality in photosynthetic PPCs which we investigate here.

Recent work in this direction has already demonstrated how the symmetry propensity of light-harvesting complex II leads to inherently efficient EET,[19] while the role of delocalized coherent exciton dynamics and localized exciton trapping has been investigated in analytical models of light-harvesting

a)Electronic mail: S.Habershon@warwick.ac.uk

systems.[20] Furthermore, extensive work has been carried out to investigate the efficiency and robustness of the Fenna-Matthews-Olson (FMO) PPC with respect to fluctuations in the protein environment, with findings showing that thermal fluctuations can enhance EET via so-called environment-assisted quantum transport (ENAQT).[21–26] Similar studies of photosynthetic systems have investigated EET efficiency optimisation with respect to environmental model parameters such as temperature or exciton trapping rates.[6,20,21,27,28] The effect of removing a chromophore on EET efficiency has also been investigated, and it has been suggested that photosynthetic EET networks display a robustness to the loss of a chromophore in the network through the utilisation of multiple EET pathways.[6,29–32]

In contrast to these previous investigations, which have focussed on the role of site energy fluctuations, environmental fluctuations, and exciton trapping rates, this article focusses predominantly on evaluating how the electronic Hamiltonian of the EET system governs the robustness and optimal EET characteristics of a biological photosynthetic system. Specifically, we adopt a network-based view of photosynthetic EET systems and focus on investigating quantum transport dynamics in a prototypical PPC, the FMO complex.[9,33–38] In green sulfur bacteria (GSB) such as *C. tepidum*,[39] FMO trimers facilitate EET from the chlorosome to the membrane-bound RC; in this process, each FMO monomer acts as an independent "molecular wiring circuit" connecting the light-harvesting antenna complex (energy source) to the RC (energy sink) (Fig. 1(a)). In recent crystal structures,[40,41] each FMO monomer comprises eight bacteriochlorophyll *a* (Bchl) chromophores embedded in a protein scaffold (Figs. 1(b) and 1(c)); Bchl sites 1, 6, and 8 (using the chromophore numbering scheme in Fig. 1(c)) are found to lie close to the chlorosome baseplate, suggesting that initial electronic excitation occurs at one of these sites (or involves an excitonic state delocalised across these chromophores[42]), while Bchl 3 is the energetic

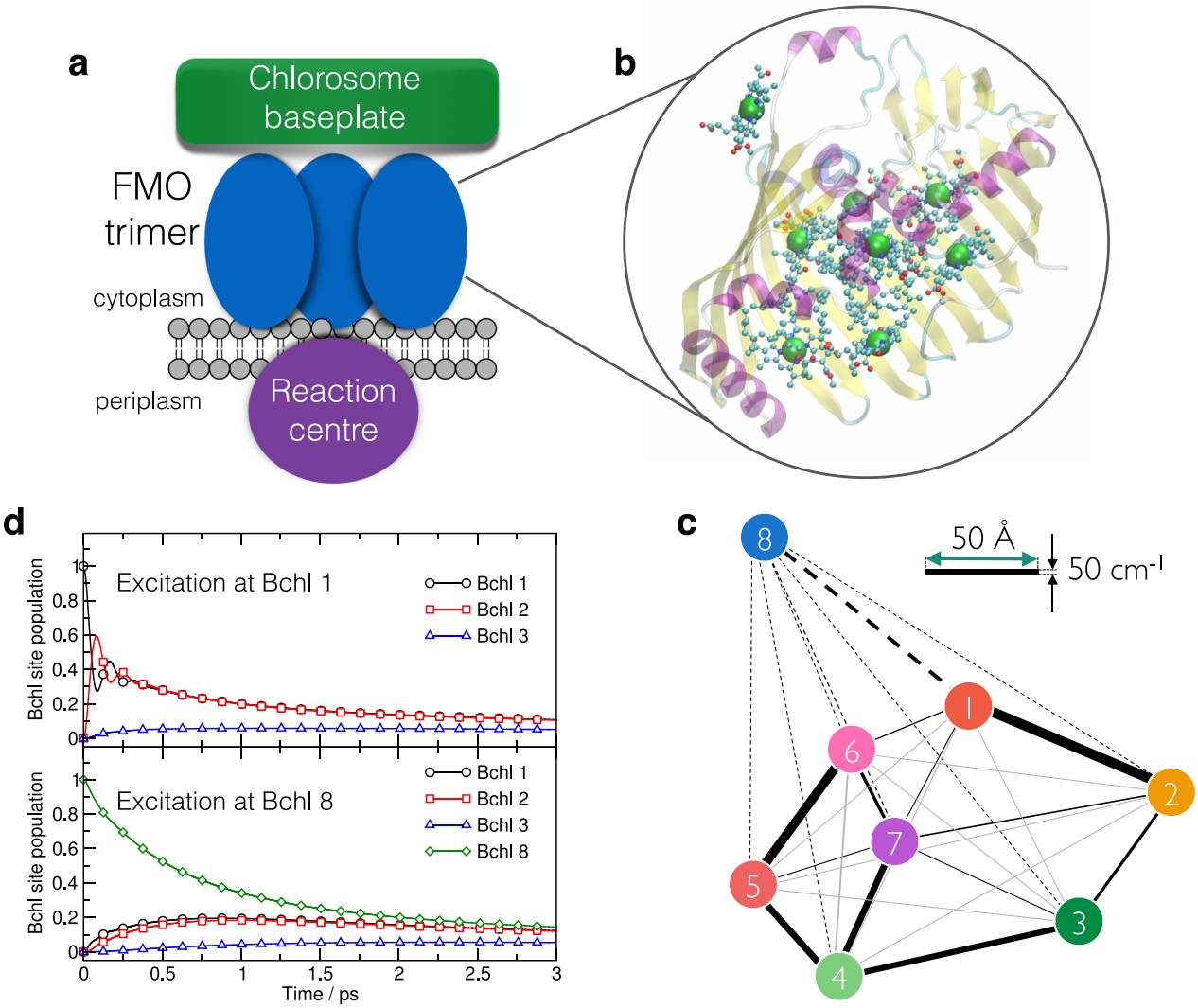

FIG. 1. (a) In GSB, FMO trimers are situated between the light-harvesting antenna complexes of the chlorosome baseplate and the trans-membrane RC. (b) Recent crystal structures of FMO[40,41] show eight Bchl chromophores embedded in a protein scaffold; here, the magnesium ions which lie at the core of each bacteriochlorophyll molecule are highlighted as green spheres. (c) Schematic diagram of the EET network in FMO, constructed using the position of magnesium ions as reference points for the relative positions of chromophores. The relative distances between chromophores are based on the crystal structure of FMO shown in (b), while the magnitude of the inter-chromophore electronic coupling elements is represented by variable line widths. (d) Typical site population dynamics determined following initial excitation at either Bchl 1 (upper panel) or Bchl 8 (lower panel).

sink in the system, funnelling electronic excitation energy to the RC. While the exact mechanism of EET to Bchl 3 is somewhat ambiguous, in part because the initial excitation in the native environment is similarly ambiguous, recent experimental and theoretical work has shown that FMO exhibits at least two different pathways for EET to site 3;[5–7,42] as we show below, these multiple transport paths, as well as the inherent heterogeneity of connectivity between different Bchl sites, are important features in maintaining robust EET.

The relative positions and orientations of Bchl sites 1 to 7 are remarkably well-conserved across GSB species,[36,43] despite differences in the amino acid sequence in the surrounding FMO protein environment;[15] furthermore, the dominant spectral characteristics of FMO complexes from different species are similarly well-conserved, falling into one of two classes which only differ due to different orientations of Bchl 8.[15] Given the conserved nature of the FMO complex in GSB, it is tempting to ask whether this particular PPC motif is in any way optimised for its EET functionality. From the point-of-view of the arrangement of Bchl sites, the answer must surely be no; it is straightforward to imagine EET networks constructed from dipole-aligned Bchl chromophores which would offer stronger inter-chromophore couplings, and hence higher EET efficiencies. This immediately suggests that there are other factors which may have driven selection of the FMO complex as the primary EET facilitator in GSB. In this article, we use quantum simulations to investigate whether any of the intrinsic properties of the Bchl chromophore network in FMO are sufficient to explain the selection of this particular light-harvesting architecture in GSB.

The remainder of this article is organized as follows. In Section II, we outline the Hamiltonian model and quantum-mechanical approach used throughout this article to simulate EET dynamics in FMO, and define a metric for EET efficiency. In Section III A, we first investigate the resilience of EET in FMO after disruptions in the chromophore interconnectivity are introduced. Remarkably, when up to 50% of the interior chromophores are removed, the EET efficiency only drops by around 20%; this decrease in efficiency is far less than that observed when a comparable number of inter-chromophore coupling elements are removed, for which the efficiency typically drops by around 90%. These results are a clear demonstration of the full extent of robustness in the EET network of FMO which goes beyond that observed previously. The results in Section III B further underline the robust nature of EET in FMO by considering the influence of environmental fluctuations in detail; specifically, we investigate how EET is influenced by both global and local chromophore environmental fluctuations. We show, for the first time, that each major EET pathway is associated with an optimal range of (global) environmental fluctuation rates; these optimal ranges do not overlap exactly, such that the overall range of environmental fluctuations over which FMO exhibits optimal efficiency is broader than if only a single EET pathway dominated. Building on these investigations of global environmental dephasing, we also investigate the influence of *local* fluctuations in environment. Specifically, we consider the distributions of EET efficiencies for an ensemble of Hamiltonians with independent Bchl site dephasing rates assigned either stochastically or biased towards non-optimal dephasing rates. The results of these simulations demonstrate that environmental-induced trapping can have a much stronger influence on EET efficiency than removing segments of the Bchl network, a factor which can be correlated with the availability of EET pathways. Furthermore, these simulations show that the source and sink sites have particular robustness to local environmental dephasing; we speculate that this effect may have a biological rationalization. Finally, in Section III C, we perform simulations for a large set of alternative FMO-like Hamiltonians in order to understand the EET optimality of FMO. We find that while it is possible to create alternative Hamiltonians which display better EET efficiency for any one initial excitation, FMO is instead one of many possible Hamiltonians which exhibit efficient EET across multiple pathways.

II. THEORY

Our treatment begins with the quantum Hamiltonian operator for the electronic sub-system of FMO; in the basis of molecular excited states, this sub-system Hamiltonian is[1,21]

$$\hat{H}_{ex} = \sum_{i=1}^{n} \epsilon_i |i\rangle\langle i| + \sum_{i<j} J_{ij} \left(|i\rangle\langle j| + |j\rangle\langle i|\right), \tag{1}$$

where ϵ_i is the electronic excitation energy of site i and J_{ij} are coupling elements between sites i and j. For the eight-site FMO network considered here (i.e., $n = 8$ in Eq. (1)), the experimental site energies are known from fluorescence studies,[42,44] while the off-diagonal couplings have been determined by the transition dipole-dipole cube method.[6]

In our treatment of the quantum dynamics of FMO-like systems, the electronic Hamiltonian of Eq. (1) is augmented by anti-Hermitian terms describing excitation energy loss by exciton recombination at each Bchl site, as well as excitonic trapping at the sink site (Bchl 3 in Fig. 1(c)).[21] Thus, the total electronic Hamiltonian operator simulated was

$$\hat{H} = \hat{H}_{ex} + \hat{H}_{trap} + \hat{H}_{rec}, \tag{2}$$

where

$$\hat{H}_{trap} = -i\hbar\kappa_3 |3\rangle\langle 3| \tag{3}$$

is the trapping operator, and

$$\hat{H}_{rec} = -i\hbar\Gamma \sum_{k=1}^{n} |k\rangle\langle k| \tag{4}$$

is the exciton recombination operator. Throughout this article, except where stated, the exciton trapping rate at Bchl site 3 is $\kappa_3 = 1\ \text{ps}^{-1}$ and the exciton recombination rate is $\Gamma = 1\ \text{ns}^{-1}$, in keeping with estimates for the *in vivo* FMO system.[21,23,45] The site energies and coupling elements of the exciton Hamiltonian $\hat{H}_{ex}$ are given in the supplementary material.[6,42,46] We note that, although Eqs. (3) and (4) are of the same form, the trapping Hamiltonian of Eq. (3) operates only at site 3, thereby giving it the characteristics of a "sink" site; in contrast, exciton recombination, as described by Eq. (4), operates on all Bchl sites.

To simulate EET dynamics in the presence of the protein environment, we use a simple quantum master equation approach which assumes that the environment induces Markovian fluctuations in all site energies, resulting in a pure dephasing effect at each Bchl site;[21,47,48] as noted in Fig. 1(d), the simulated site population dynamics from this simple model are qualitatively consistent with more complex theoretical approaches. For example, qualitatively good agreement in population dynamics is observed compared to the Hierarchical Equation-Of-Motion (HEOM),[8,9] the Generalized Bloch-Redfield (GBR) method,[6] or Linearized Semiclassical Initial Value Representation (LSC-IVR).[49,50] Furthermore, we note that the main interest of this work is in assessing the impact of modifying gross features of the electronic sub-system, such as the number of chromophores present; it might reasonably be expected that such trends would be qualitatively reproduced by a simple dephasing mode, and only mildly influenced by explicit correlation with the environment. Finally, we note a practical limitation; in this work, we performed around 100×10^3 independent simulations of perturbed FMO-like Hamiltonians, a feature which clearly demands a computationally tractable treatment.

The equation-of-motion for the elements of the density matrix, written in the basis of molecular excited states, is

$$\frac{d\rho_{ij}(t)}{dt} = \mathcal{H}[\rho]_{ij} + \mathcal{L}[\rho]_{ij}, \tag{5}$$

where

$$\mathcal{H}[\rho]_{ij} = -\frac{i}{\hbar}\left[\hat{H}, \hat{\rho}(t)\right]_{ij} \tag{6}$$

is the usual time-derivative of the density matrix. The factor $\mathcal{L}[\rho]_{ij}$ is a functional which models the interaction of the electronic sub-system with the protein environment; here, this is given by a pure dephasing effect, and $\mathcal{L}[\rho]_{ij}$ is of the form

$$\mathcal{L}[\rho]_{ij} = -\left(\frac{1}{2}(\gamma_i + \gamma_j) - \sqrt{(\gamma_i\gamma_j)\delta_{ij}}\right)\rho_{ij}, \tag{7}$$

where γ_i is the dephasing rate at site i. In the large majority of the calculations reported here, unless otherwise stated, we assume that the dephasing rate is the same at all Bchl sites, with $\gamma_i = 100$ cm^{-1}.[21,23,45] This value lies well within the environment-assisted quantum transport regime.[21] Furthermore, as discussed in detail in Section III B, the EET efficiency of FMO is surprisingly robust to the exact value of the dephasing rate within a window from 40 cm^{-1} to 3000 cm^{-1}. Unless otherwise stated, we adopt the standard assumption that all sites experience the same (global) dephasing rate; the role of local variations in dephasing rates is discussed explicitly in Section III B. Finally, we note in passing that singlet-singlet annihilation can have an important role to play in FMO under high-intensity light conditions,[51] although our simulations follow related work in operating under the standard assumption that the light intensity in the system is low enough that singlet-singlet annihilation can be ignored.

To quantify the efficiency of EET to the RC via Bchl site 3, we calculate the time-integral of the population at site 3,[21]

$$\eta = 2\kappa_3 \int_0^{t_{\max}} \rho_{33}(t)\, dt, \tag{8}$$

where $t_{max} = 10$ ps. This value of t_{max} is sufficiently long to capture the dominant population dynamics at the Bchl sites as the natural time scale for EET population transfer dynamics is of the order of $\sim\frac{1}{\kappa_3} = 1$ ps.[23] Furthermore, in this article we consider a range of artificial Hamiltonians with dynamics which may be slower than FMO, thus this time scale will be sufficient for a range of different Hamiltonians. All of our calculations employed a standard fourth-order Runge-Kutta algorithm[52] to integrate the equations-of-motion for the density matrix elements; a time-step of 0.5 fs was used throughout.

Given the matrix representation of the electronic Hamiltonian, the connection to the mathematical theory of graphs (or networks) is evident. In particular, the matrix representation of the Hamiltonian can be viewed as representing the weighted adjacency matrix of an undirected graph;[53,54] each of the eight Bchl sites represents a graph node (or vertex), with the graph edges representing the interactions which couple different chromophores. This network-based view of FMO's PPC is particularly useful in understanding robustness and efficiency of EET, as shown below.

III. RESULTS AND DISCUSSION

The electronic Hamiltonian of Eq. (1), along with a simple description of environment-induced relaxation, provides a straightforward method to investigate the influence of both chromophore network and protein environment in FMO-like systems. We particularly focus on the resilience of the FMO EET network to changes in Bchl organisation and environmental relaxation, before discussing the EET efficiency landscape of FMO-like systems.

A. Robustness to network change

Given the conserved nature of FMO across GSB species, we first investigate network robustness; in other words, how resilient is transport in FMO to changes in the connectivity of the EET network? In the context of network theory, network robustness can be systematically investigated by assessing the impact of deleting nodes and edges.[53] In the FMO network, these perturbations correspond to removal of Bchl chromophores (and related couplings) or removal of individual inter-site coupling elements; the former may arise from transcription errors or mutations in the genes responsible for signalling FMO production, while the latter may result from localised environmental perturbations which disrupt the relative orientations and/or distances of a given pair of chromophores. As a result, assessing the EET efficiency of perturbed FMO-like networks provides a route to assess the robustness of the photosynthetic apparatus in GSB organisms; as shown below, these results also provide detailed insight into the mechanism of EET in FMO.

Figure 2(a) shows the effect on transfer efficiency (see the supplementary material[46]) of removing Bchl sites from the FMO network, excluding the source and trap sites; initial excitations at sites 1, 6, and 8 are considered. In these calculations, *all* possible combinations of chromophores are selected to be removed for a given removal number, and the resulting efficiencies of the generated networks are averaged to obtain the results shown; for example, in the calculations where just two chromophores are removed, all possibilities of chromophore pairs are considered, excluding removal of source and sink sites.

We find that even when three Bchl sites are removed, representing 50% of the sites which are neither sink nor source, the EET efficiency arising from excitation at site 1 or 6 decreases by only around 20% compared to that of the original full network; thus, FMO appears to demonstrate a high degree of robustness to changes in the *nodes* of the EET network. To our knowledge, this is the first time that the full extent of the robust nature of FMO to chromophore network disruption has been determined. In contrast, Fig. 2(b) demonstrates that FMO is much less robust to the removal of randomly chosen *edges*; after removing 18 edges, which is the same number removed when three chromophores (nodes) are removed in Fig. 2(a), the EET efficiency drops to around 10% of the original values.

As an aside, it is interesting to consider the influence of the Bchl 3 trapping rate, κ_3, on the observed EET efficiencies and their response to chromophore removals. As noted above, while an experimental value for κ_3 is difficult to ascertain, previous simulation work for FMO has demonstrated that trapping rates on the order of 1-10 ps^{-1} result in efficient EET and low transfer time scales; furthermore, these values are sufficiently fast that exciton recombination, occurring at a typical rate of 1 ns^{-1}, is effectively avoided. To investigate the influence of a slower trapping rate, Fig. 2(c) illustrates EET efficiencies determined in the same way as in Fig. 2(a), but with a trapping rate of $\kappa_3 = 1$ ns^{-1}. We find a similar trend to that observed in Fig. 2(a), with the FMO network

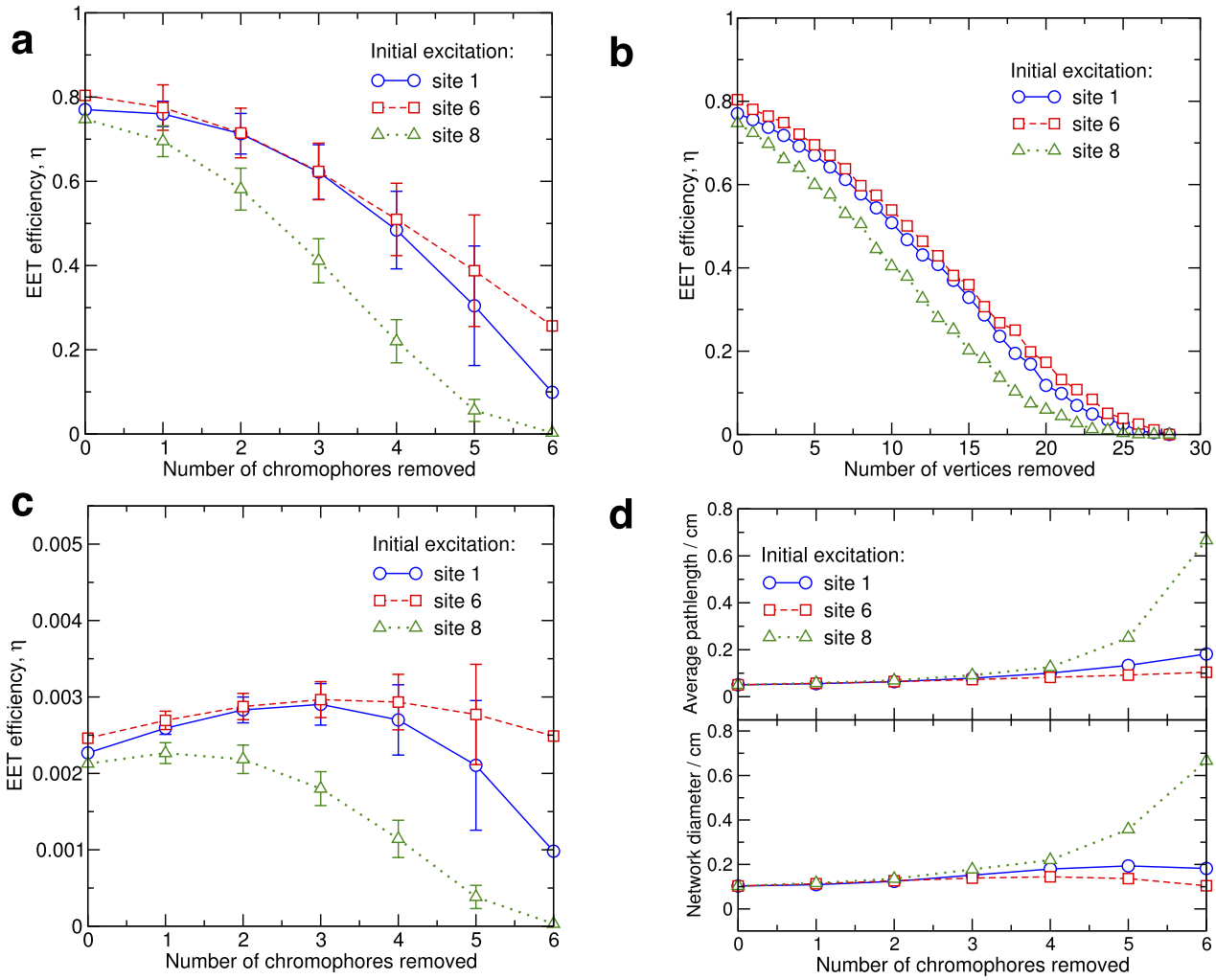

FIG. 2. (a) EET efficiency for a series of FMO Hamiltonians in which increasing numbers of Bchl sites, as well as the corresponding coupling elements, are removed. (b) A similar "knockout" study can be performed by removing random edges from the FMO network, rather than Bchl sites; in this case, the FMO EET network is easily disrupted because random removals are more likely to disrupt several EET pathways simultaneously. Each result shown here is averaged over 1000 different "knockout" Hamiltonians; the final error bars are comparable in size to the symbols. (c) EET efficiencies for FMO-like systems, as determined in panel (a), but with a trapping rate of 1 ns^{-1} rather than 1 ps^{-1}. (d) Upon removal of chromophores from the FMO network, the average path-length between nodes (upper panel; excluding source and sink nodes) was calculated using the Floyd-Warshall algorithm[57,58] with inter-node distances defined as $d_{ij} = |J_{ij}|^{-1}$; the network diameter, shown in the lower panel, is the largest observed inter-node "path-length" for each network size.

demonstrating robustness to chromophore removal; however, in Fig. 2(c), this robustness is more prominent. The difference arises because the faster trapping rate (Fig. 2(a)) more strongly distinguishes between different pathways through the network. In other words, paths which result in good population transfer to site 3 (see below) will be more strongly distinguished from those which result in poorer population transfer to site 3, simply by virtue of the fact that the trapping influences site 3 only. In the case of slow trapping rate (Fig. 2(c)), the distinction between different paths is only weakly influenced by the trapping rate, with the more important factor being the intrinsic properties of the network itself, as discussed below.

How does the robustness to chromophore removal arise? The key to answering this question lies in the existence of *multiple* EET pathways through the FMO electronic network. Previous simulations have also demonstrated this feature of FMO,[6,9,55] although the existence of multiple robust EET pathways in FMO is particularly straightforward to demonstrate in our network-based view. In particular, Fig. 2(d) shows the average path-lengths between all pairs of nodes (excluding source and sink), as well as the longest path-length in the network; both factors are standard measures of node connectivity in a network. In our calculations, the path-lengths are defined such that stronger Bchl interactions (large $|J_{ij}|$) correspond to "shorter" paths; as a result, our calculated path-lengths reflect the strength of electronic couplings along different paths. Figure 2(d) clearly shows that both of these measures of network connectivity are essentially unaffected by the removal of Bchl chromophores, particularly for excitations at Bchl 1 and Bchl 6; even in the case of Bchl 8, more than 4 Bchl sites must be removed before significant changes in electronic coupling strengths along path-lengths are observed. The conclusion from Fig. 2(d) is that network resilience (Figs. 2(a) and 2(c)) is a consequence of *heterogeneity* of dynamic paths in the EET network; in other words, several strongly coupled electronic pathways connect any given pair of nodes, leading to a robust network which requires large-scale disruption to halt EET completely. The existence of multiple pathways is also supported by Fig. 2(b); while removal of nodes and related edges will leave alternative pathways for EET open, removal of *random* edges can simultaneously disrupt many EET paths, leading to a much more severe decrease in efficiency.

The presence of multiple EET pathways in FMO is further emphasised in Fig. 3. For each initial excitation site, major EET pathways can be identified by evaluating the transport efficiency after removal of inter-chromophore coupling elements J_{ij}; removing couplings which are strongly involved in EET from a given initially excited site results in a significant drop in efficiency. This approach can be extended to removing multiple coupling elements (as shown in the supplementary material[46]), allowing identification of the dominant EET paths in the system. This "knockout" analysis clearly shows multiple EET pathways in FMO; the most dominant are given in Fig. 3. We find that excitation at sites 1 and 6 each exhibits two major EET paths, while excitation at Bchl 8 exhibits one dominant path as a result of weak electronic coupling between Bchl 8 and all others except Bchl 1. These paths are consistent with previous work which has, for example, identified at least two major contributing paths;[6] however, the most important point is that our "knockout" analysis clearly shows a multitude of EET paths through FMO which contribute to EET to differing extents.

The conclusion from these simulations is that the FMO EET network is surprisingly robust to changes in the Bchl site connectivity; removing 50% of the network has only a

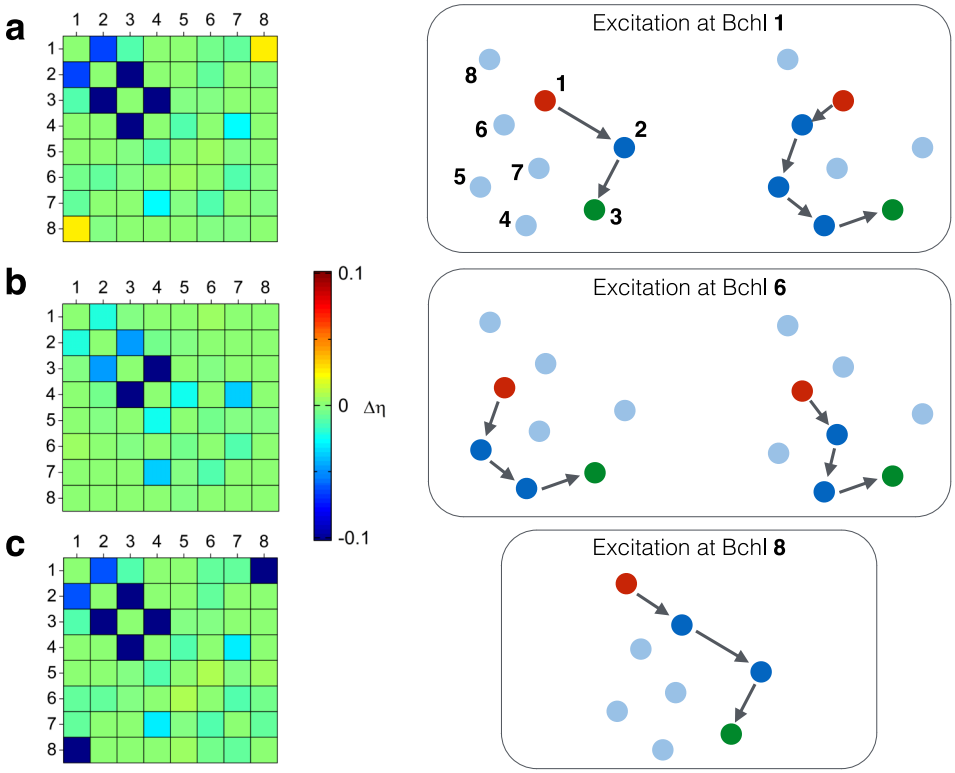

FIG. 3. Dominant EET pathways following excitation at (a) Bchl 1, (b) Bchl 6, and (c) Bchl 8. The grids on the left illustrate the effect of removing single inter-chromophore coupling elements J_{ij} on the calculated EET efficiency, relative to the original FMO Hamiltonian ($\Delta\eta$); warm colours indicate an increase in efficiency, while cool colours label those sites which cause a decrease in efficiency and are therefore more important to the dominant EET pathways in each case. The axes label the indices of the coupling element which has been removed from the original FMO Hamiltonian.

relatively small impact on EET efficiency, particularly when compared to removing a similar number of random edges. Although the impact of removing a single chromophore has been noted previously,[30] the present work is the first to reveal the full extent of FMO EET robustness to disruption in the chromophore network. Furthermore, this is the first time that a simple network-based view, focussing on average and longest path-lengths, has been used to rationalise this feature. The EET efficiency in FMO is underpinned by a multitude of transport pathways, such that removal of individual Bchl sites, for example, by chemical or photochemical damage, simply diverts EET along an alternative path of similar electronic coupling strength. This behaviour is in contrast to many biological networks, which are often found to be scale-free in a similar fashion to the world wide web;[53] instead, the compact, fully connected nature of inter-chromophore coupling in FMO provides a surprising degree of network resilience in support of EET.

B. Robustness to environmental noise

1. Efficiency of EET with a global dephasing rate

The results of Figs. 2 and 3 demonstrate that FMO is strongly robust to disruption of the Bchl network, but what about the role of environmental perturbations? Several GSB species are known to be thermophilic; for example, *C. tepidum* is found in hot springs at temperatures of up to 52 °C.[39] However, the crystal structures of the FMO complex derived from thermophilic and non-thermophilic GSB are very similar,[15,36,43] suggesting that the FMO complex is sufficiently robust to changes in the thermal fluctuations of the protein environment such that no special adaptations are necessary. Here, we investigate this environmental resilience in the light of the inherent heterogeneity of the FMO network observed above. Here we consider a global dephasing rate such that each site experiences the same dephasing $\gamma = \gamma_i$ in Eq. (7); in other words, the interaction between the Bchl network and the environment was assumed to be the same at each Bchl site. The calculations performed above employed a single *global* dephasing rate representing the influence of the environment; in other words, the interaction between the Bchl network and the environment was assumed to be the same at each Bchl site. In this section, we investigate the interplay between environmental noise and multiple EET paths; below we expand these simulations to consider the role of independent local dephasing rates.

Figure 4 shows the effect of changing global environmental fluctuations; these fluctuations give rise to pure dephasing in our simple description of the density matrix dynamics, with large dephasing rates approximating the influence of a strongly perturbative environment, as might be found at elevated temperatures. These calculations were performed for the full 8-site FMO electronic Hamiltonian; only the global dephasing rate $\gamma = \gamma_i$ in Eq. (7) was modified.

It is clear from Fig. 4 that excitations at Bchl 1 and 6 show little change in efficiency as the dephasing rate changes over two orders-of-magnitude from 40 cm^{-1} to around 3000 cm^{-1}, whereas EET transport decreases strongly outside this range.

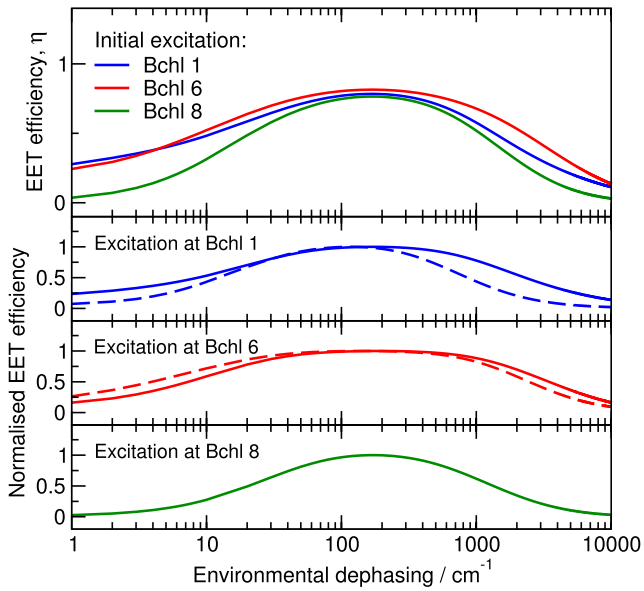

FIG. 4. Role of global environmental dephasing rate. The top panel shows the effect of environmental dephasing rate, γ, on the calculated EET efficiency, η for excitation at Bchl sites 1, 6, and 8; notably, efficient transport from sites 1 and 6 is maintained over approximately two orders-of-magnitude in the dephasing factor. Excitation at site 8 is somewhat more susceptible to environmental noise, most likely a result of the weaker coupling between Bchl 8 and the remaining chromophores.

This environmental-assisted quantum transport phenomenon has been noted in previous simulations of a seven-site FMO model;[21] weak dephasing results in oscillatory populations with little effective transport, while strong dephasing results in exciton localisation. Excitation at Bchl 8 is less resilient to changes in the dephasing rate, as might be expected as a result of the weaker coupling with the remaining chromophores.

What is particularly interesting about these results is how they relate to the multiple EET pathways observed above; we find that the broad spectral range over which EET is efficient arises because different EET pathways have different responses to environmental perturbations. This is highlighted in the lower panels of Fig. 4, which shows the dephasing rate dependence of EET for the five major pathways shown in Fig. 3. For these calculations, the sites which do not form part of the specified EET pathway are removed from the Hamiltonian; for example, for the pathway $1 \rightarrow 2 \rightarrow 3$, chromophore sites 4, 5, 6, and 8 are removed from the network and the transfer efficiency across the range of dephasing rates is calculated. However, it is important to note here that the *absolute* EET efficiencies in systems containing just a single pathway will be greater than the full FMO Hamiltonian by virtue of the absence of competing pathways; instead, we focus our attention here on the spectral (i.e. frequency) range of environmental response for the normalised efficiencies.

Particularly for excitation at Bchl 1 and 6, we find that the two different paths of Figs. 3(a) and 3(b) exhibit distinct responses to the environment which are centered at different dephasing rates. For example, the $1 \rightarrow 2 \rightarrow 3$ pathway has a well-defined peak at around 130 cm^{-1}, whereas the $1 \rightarrow 6 \rightarrow 5 \rightarrow 4 \rightarrow 3$ pathway displays a peak at a slightly shifted value of 300 cm^{-1}. As a result of the environmental response of different pathways being centered

on different dephasing rates, the transport efficiency of FMO is maintained across a much wider range of dephasing rates (or environmental conditions) than would be possible if only one EET pathway operated. We conclude, as above, that the network heterogeneity of FMO is a key feature, in this case giving rise to significant robustness against environmental change.

2. Efficiency of EET with local dephasing rates

The simulations above employed a single global dephasing rate to model environmental interactions at each Bchl site. We now investigate EET dynamics in the presence of different dephasing rates at each Bchl site, representing different local fluctuations in site environments.

We first investigate the general role of heterogeneous dephasing rates on EET efficiency. Here, we generated 2×10^3 model Hamiltonians in which the EET system Hamiltonian was identical to that in FMO, but the dephasing rates γ_i are independently sampled from a log-uniform probability distribution in the range $\gamma_i \in [1\ \text{cm}^{-1}, 10\,000\ \text{cm}^{-1}]$; as before, the corresponding EET efficiency was calculated for initial excitations at sites 1, 6, and 8.

Figure 5 shows the histogram of EET efficiencies calculated for these 2×10^3 realisations of local dephasing. These distributions show a characteristic skew towards lower efficiency values; given the previous results concerning the range of dephasing rates which give rise to efficient EET, this is perhaps not surprising. In particular, we find that those sets of dephasing rates which give rise to lower EET efficiency than simulations employing a single global dephasing rate of 100 cm^{-1} tend to have "poor" dephasing rates (i.e., 100 $\text{cm}^{-1} > \gamma > 3000\ \text{cm}^{-1}$) for Bchl sites which contribute to the dominate EET pathways for the given initial excitation. This is a clear demonstration of the role of local exciton trapping in EET efficiency, as noted previously.[20]

In contrast, for those Hamiltonians which give rise to enhanced EET (relative to FMO with a global dephasing rate of 100 cm^{-1}), the set of local dephasing rates are found to have common features: (i) sites which are *not* part of the dominate EET pathway for a given initial excitation (Fig. 3) have dephasing rates which lie outside the robust region identified in Fig. 4 and (ii) sites which form the dominate EET pathway have dephasing rates well within the robust region of Fig. 4. While these results are consistent with previous analyses of simpler EET networks,[20] our findings show that similar

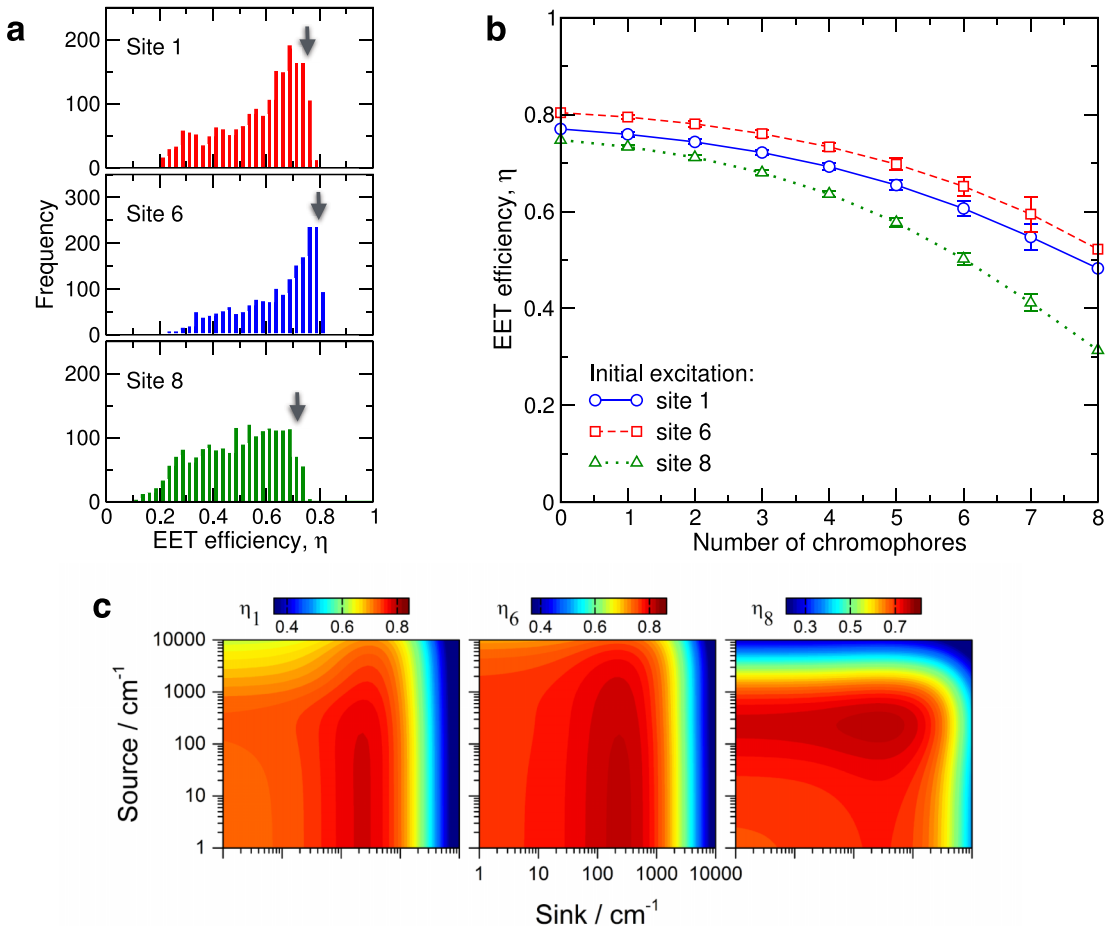

FIG. 5. (a) EET efficiency histograms for 2×10^3 FMO-like Hamiltonians with randomly sampled local dephasing rates; results are shown for initial excitation at sites 1, 6, and 8. The arrows indicate the efficiency of the FMO model with a global dephasing rate of 100 cm^{-1}. (b) EET efficiencies calculated in simulations in which increasing numbers of Bchl sites are given a "poor" dephasing rate of 10 cm^{-1}; in each case, all possible combinations are generated and the EET efficiencies are averaged. (c) EET efficiencies as a function of local dephasing rate at source and sink (Bchl 3) sites; results are shown for initial excitations at site 1 (left), site 6 (centre), and site 8 (right).

considerations of EET optimisation, particularly balancing of coherent exciton transport and local exciton trapping, are equally valid in more complex light-harvesting systems.

In a second investigation of the role of local dephasing, Fig. 5(b) also shows the influence of assigning different numbers of chromophore sites "poor" local dephasing rates (as defined above); as in Fig. 2(a), we considered all possible combinations of sites in these "dephasing knockout" experiments. We chose to assign a dephasing rate of 10 cm^{-1} to those Bchl sites selected to have "poor" dephasing rates, with the remaining Bchl sites maintaining a value of $\gamma_i = 100\ cm^{-1}$. The resulting efficiencies of the networks with sites are averaged to obtain the results shown in Fig. 5(b). The results indicate a monotonically decreasing EET efficiency as the number of Bchl sites with "poor" dephasing rate increases; this is clearly consistent with the results of Fig. 5(a), which demonstrated that the probability of generating a Hamiltonian with a reduced efficiency (relative to FMO with a single global dephasing rate of 100 cm^{-1}) is high.

Finally, we investigate the effect of changing the dephasing rate for source and sink sites only; the rationale for this set of simulations is that these sites lie on the exterior of the FMO protein, and hence are most likely to experience environmental dephasing rates which are different from those Bchl sites lying on the interior of FMO. In these calculations, all interior sites were given the same dephasing rate of 100 cm^{-1}, and the source and sink site dephasing rates were varied in the range 1-10 000 cm^{-1}; the resulting EET efficiencies determined in these simulations are shown in Fig. 5(c). We find that initial excitations at sites 1 and 6 are relatively insensitive to the source dephasing rate but demonstrate a much greater dependence on the sink (Bchl 3) dephasing rate. In contrast, initial excitation at site 8 is dependent on both the source and sink dephasing rates; in particular, there is a clear range of dephasing rates for which EET is optimal. These results can be understood with reference to Fig. 1. In particular, initial excitation at sites 1 and 6 results in a rapid initial decay of population which is almost complete after around 1 ps; in contrast, initial excitation at site 8 results in a much slower incoherent decay profile, as discussed in more detail below. As a result of these slower population transfer characteristics, it is not surprising that site 8 may be more strongly influenced by local exciton trapping. These results serve to underline the interplay between EET efficiency, electronic network characteristics, and environmental dephasing in modulating EET efficiency.[20]

C. Efficiency of EET in FMO-like networks

Our simulations so far have shown the extent to which FMO is resilient to changes in both the electron EET subsystem and the characteristics of the protein environment on both a global scale and at the local Bchl scale; the final question we address here is whether FMO is in any way optimised with respect to the efficiency of EET. It is not difficult to see that a very efficient EET network could be built as a simple linear system containing a few strongly coupled chromophores.[29,56] While this might result in efficient and rapid EET, we must bear in mind that the RC performs charge-separation reactions at a rate of about 1 ps^{-1}, so ensuring that excitation energy is transferred to the RC any faster than this time scale is essentially useless. Furthermore, such a linear arrangement involving few chromophores would lack any of the network robustness which we have emphasised above; removing a single chromophore would break the EET path and disable transport.

Bearing this in mind, we limit ourselves to assessing whether FMO is optimally efficient amongst other possible eight chromophore FMO-like networks; after all, FMO is well-conserved across GSB species.[15,36,39,43] In particular, we generate 2×10^3 alternative eight-site electronic Hamiltonians by adding Gaussian random noise to all elements of the FMO Hamiltonian (see the supplementary material[46]). We note the possibility that some Hamiltonians generated in this manner may be physically unrealistic; however, in general, this approach allows us to generate Hamiltonians which are representative of FMO complexes with modified inter-chromophore distances and relative molecular orientations, as well as electronic changes at the Bchl sites themselves.

For each generated FMO-like Hamiltonian, we determine the EET efficiency for excitations at Bchl sites 1, 6, and 8. The results are shown in Fig. 6(a), plotted against the range (Q) of calculated efficiencies; note that the range is simply the difference between the largest and smallest calculated efficiency values following excitation at Bchl sites 1, 6, and 8, for each Hamiltonian considered. We observe a clear trend in the EET efficiencies; those networks exhibiting the largest efficiencies do so for excitation at Bchl sites 1 and 6, at the expense of low EET efficiency from site 8. Further analysis shows that many of these networks are characterised by large site energies at Bchl 8, as illustrated in Fig. 6(b). As shown previously,[6] and in Fig. 1(d), the population dynamics arising from initial excitation at Bchl site 8 are characterised as a slow incoherent decay, the time scale of which only increases as the Bchl 8 site energy increases; this is confirmed in the population dynamics of a FMO-like Hamiltonian with a low EET efficiency for excitation at Bchl 8. In contrast, those networks which exhibit similar EET efficiencies for all initial excitations are characterised by smaller values of the Bchl 8 site energy along with strong electronic couplings along at least one of the pathways involving Bchl 1 or 6; again, this is illustrated in Fig. 6.

Most interestingly, the original FMO Hamiltonian sits at $Q \simeq 0.05$, where EET efficiency is similar for all initial excitations. In other words, while it is possible to generate FMO-like networks with better EET efficiency for initial excitation at any *one* of the Bchl sites 1, 6, and 8, FMO's network and chromophore characteristics result in simultaneously good EET efficiency for *all* initial excitations considered here. Given that the initial exciton generated *in vivo* is most likely to be delocalised across several Bchl sites, this characteristic of FMO appears to be desirable over optimal efficiency for a specific excitation. As a final point, we note that our approach to generating alternative FMO-like Hamiltonians limits us to exploring a finite set of all possibilities, although we suggest that these are the chromophore arrangements which would be allowed given the constraints of the FMO protein environment; simulations

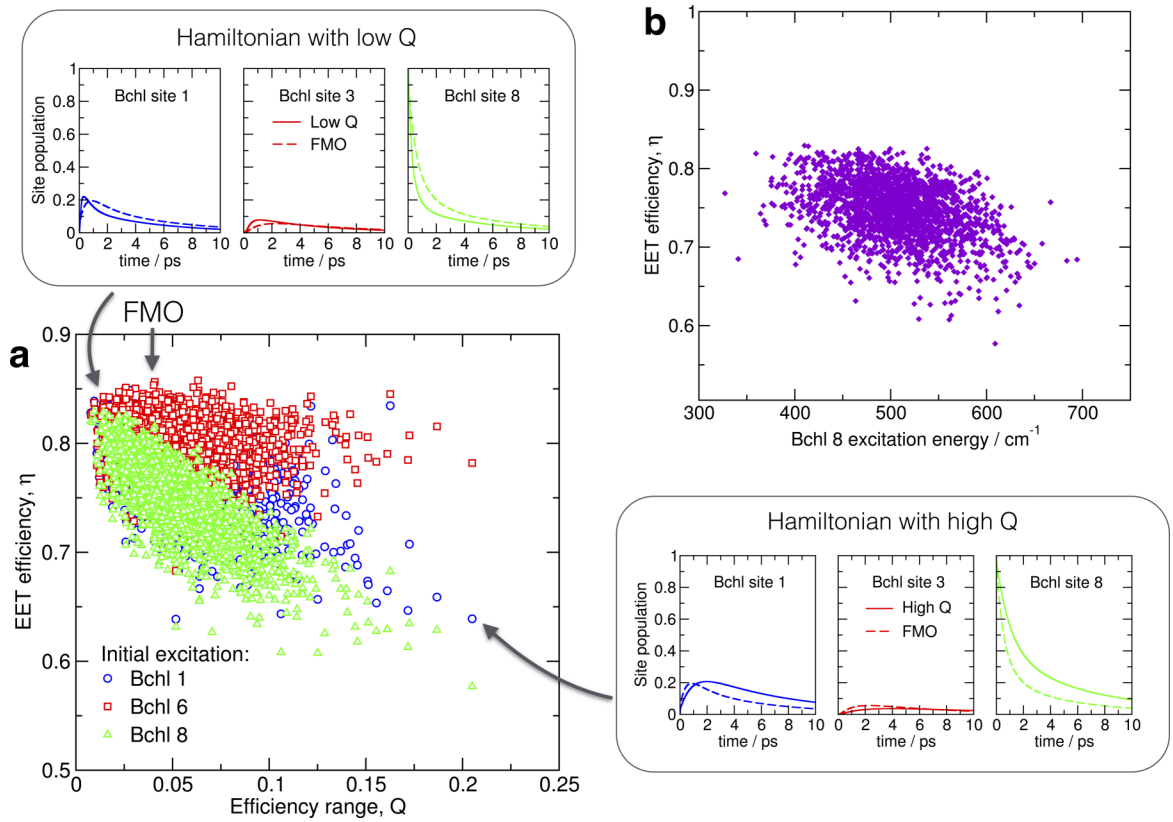

FIG. 6. (a) EET efficiency of 2×10^3 FMO-like electronic Hamiltonians generated by adding Gaussian random noise to the original 8-site FMO Hamiltonian. The x-axis plots the range, Q, calculated using the EET efficiency resulting from initial excitation at Bchl 1, 6, and 8; the original FMO model is found at $Q \simeq 0.05$. The upper-left panel shows the population dynamics at Bchl 1, 3, and 8 for a Hamiltonian with a small Q value (similar efficiency for all initial excited-states) following excitation at site 8. As is typical for such Hamiltonians, the site energy of Bchl 8 is comparable to the original FMO model and the inter-chromophore coupling strengths are, in general, slightly stronger than FMO; as a result, the population of site 8 decreases much faster than FMO. In contrast, the panel at lower-right shows the results for a Hamiltonian with large Q value; here, the site energy of Bchl 8 is much larger than that of site 1 and the incoherent decay of population is much slower than in FMO. (b) Plotting EET efficiency from site 8 against the Bchl 8 site energy emphasises the role of this parameter in determining the network efficiency characteristics.

aimed at exploring a much wider structural space are under way.

IV. CONCLUSIONS

For the first time, the full extent of FMO robustness has been revealed and rationalised by combining quantum simulations with a network-based view of EET. We have demonstrated several important features of this prototypical EET system. A major conclusion from this work is revealing the *extent* of which EET efficiency in FMO is robust to changes in both the chromophore network and the environmental fluctuations, factors which may help explain why FMO is conserved across GSB species which experience a range of physiological conditions. In particular, we find that EET in FMO is robust to removal of up to 50% of the interior chromophore sites, predominantly as a result of the presence of multiple EET pathways as demonstrated in network-based calculations. We have also shown that EET is robust to environmental fluctuations across a broad range of dephasing rates, and have demonstrated that this broad response may be a result of the different environmental response of different EET pathways. Finally, we have considered in detail the role of local dephasing rates; our simulations are consistent with previous investigations of the role of exciton trapping, but have also singled out the different role of dephasing at the source and sink sites.

Interestingly, we find that similar EET transport is observed after initial excitation at any of Bchl sites 1, 6, or 8; this is a particularly appealing feature given that the initial excited state is expected to be delocalised over the chromophores adjacent to the chlorosome baseplate. We emphasise that a key underlying feature which enables these properties is the network heterogeneity, which gives rise to multiple transport paths from source to sink sites. Finally, we have shown that the site energy of Bchl 8 is a particularly important determinant of EET efficiency. It is interesting to note that a bi-exponential fit to the population decay following excitation at Bchl 8 in FMO gives a component with a time-constant of around 2.5 ps, comparable to the reaction rate at the RC;[21,23] as a result, the Bchl 8 site energy seems to be tuned to provide EET at a sufficient rate, and no more. Understanding the extent to which these network characteristics are observed in other photosynthetic systems is a goal of current work.

As a final point, we note that, although our simulations have revealed interesting network characteristics, we are of course limited in the extent to which the properties of FMO can be understood in the wider biological context. For example, we cannot rule out the fact that FMO may be the dominant PPC in GSB simply because it is easily

synthesised from readily available molecular building blocks; in fact, sequence alignment suggests that the FMO protein is related to PscA, a protein found in the RC of GSB, perhaps suggesting that the organisation of Bchl in the FMO complex is a simple consequence of arrangement into a pre-existing, and synthetically accessible protein framework.[34] Taken together, this work suggests that chromophore molecular characteristics and organisation, protein framework and synthetic accessibility may all play a role in the ultimate viability of light-harvesting molecular architectures, factors which might be carried over to design of new artificial photosynthetic systems.

ACKNOWLEDGMENTS

The authors are grateful to the EPSRC Doctoral Training Centre *Molecular Organisation and Assembly in Cells* (Grant No. EP/F500378/1) for funding, and to the Centre for Scientific Computing at the University of Warwick for providing computational resources.

[1]Y.-C. Cheng and G. R. Fleming, Annu. Rev. Phys. Chem. **60**, 241 (2009).
[2]N. Lambert, Y. Chen, Y. Cheng, C. Li, G. Chen, and F. Nori, Nat. Phys. **9**, 10 (2013).
[3]G. D. Scholes, G. R. Fleming, A. Olaya-Castro, and R. van Grondelle, Nat. Chem. **3**, 763 (2011).
[4]D. Abramavicius and S. Mukamel, J. Chem. Phys. **133**, 064510 (2010).
[5]J. Adolphs and T. Renger, Biophys. J. **91**, 2778 (2006).
[6]J. Moix, J. Wu, P. Huo, D. Coker, and J. Cao, J. Phys. Chem. Lett. **2**, 3045 (2011).
[7]G. S. Engel, T. R. Calhoun, E. L. Read, T.-K. Ahn, T. Mancal, Y.-C. Cheng, R. E. Blankenship, and G. R. Fleming, Nature **446**, 782 (2007).
[8]A. Ishizaki and G. Fleming, Proc. Natl. Acad. Sci. U. S. A. **106**, 17255 (2009).
[9]A. Ishizaki and G. Fleming, Annu. Rev. Condens. Matter Phys. **3**, 333 (2012).
[10]G. D. Scholes, J. Phys. Chem. Lett. **1**, 2 (2010).
[11]V. Sündstrom, Annu. Rev. Phys. Chem. **59**, 53 (2008).
[12]M. Sarovar, A. Ishizaki, G. Fleming, and K. Whaley, Nat. Phys. **6**, 462 (2010).
[13]R. van Grondelle and V. I. Novoderezhkin, Phys. Chem. Chem. Phys. **8**, 793 (2006).
[14]J. M. Olson and R. E. Blankenship, Photosynth. Res. **80**, 373 (2004).
[15]R. Blankenship, Plant Physiol. **154**, 434 (2010).
[16]S. Y. Reece, J. A. Hamel, K. Sung, T. D. Jarvi, A. J. Esswein, J. J. H. Pijpers, and D. G. Nocera, Science **334**, 645 (2011).
[17]W. E. Piers, Organometallics **30**, 13 (2011).
[18]R. E. Blankenship, D. M. Tiede, J. Barber, G. W. Brudvig, G. Fleming, M. Ghirardi, M. R. Gunner, W. Junge, D. M. Kramer, A. Melis, T. A. Moore, C. C. Moser, D. G. Nocera, A. J. Nozik, D. R. Ort, W. W. Parsons, R. C. Prince, and R. T. Sayre, Science **232**, 805 (2011).
[19]L. Cleary, H. Chen, C. Chuang, R. J. Silbey, and J. Cao, Proc. Natl. Acad. Sci. U. S. A. **110**, 8537 (2013).
[20]J. Cao and R. J. Silbey, J. Phys. Chem. A **113**, 13825 (2009).
[21]P. Rebentrost, M. Mohseni, I. Kassal, S. Lloyd, and A. Aspuru-Guzik, New J. Phys. **11**, 1 (2009).
[22]S. F. Huelga and M. B. Plenio, Contemp. Phys. **54**, 181 (2013).
[23]M. Mohseni, P. Rebentrost, S. Lloyd, and A. Aspuru-Guzik, J. Chem. Phys. **129**, 174106 (2008).
[24]P. Rebentrost, M. Mohseni, and A. Aspuru-Guzik, J. Phys. Chem. B **113**, 9942 (2009).
[25]I. Kassal and A. Aspuru-Guzik, New J. Phys. **14**, 053041 (2012).
[26]A. W. Chin, A. Datta, F. Caruso, S. F. Huelga, and M. B. Plenio, New J. Phys. **12**, 065002 (2010).
[27]T. Scholak, F. de Melo, T. Wellens, F. Mintert, and A. Buchleitner, Phys. Rev. E **83**, 021912 (2011).
[28]J. Wu, F. Liu, Y. Shen, J. Cao, and R. J. Silbey, New J. Phys. **12**, 105012 (2010).
[29]J.-H. Kim and J. Cao, J. Phys. Chem. B **114**, 16189 (2010).
[30]J. Wu, F. Liu, J. Ma, R. J. Silbey, and J. Cao, J. Chem. Phys. **137**, 174111 (2012).
[31]G.-Y. Chen, N. Lambert, C.-M. Li, Y.-N. Chen, and F. Nori, Phys. Rev. E **88**, 032120 (2013).
[32]M. K. Sener, D. Lu, T. Ritz, S. Park, P. Fromme, and K. Schulten, J. Phys. Chem. B **106**, 7948 (2002).
[33]R. E. Fenna and B. W. Matthews, Nature **258**, 573 (1975).
[34]J. M. Olson and J. Raymond, Photosynth. Res. **75**, 277 (2003).
[35]Y.-F. Li, W. Zhou, R. E. Blankenship, and J. P. Allen, J. Mol. Biol. **271**, 456 (1997).
[36]A. Camara-Artigas, R. E. Blankenship, and J. P. Allen, Photosynth. Res. **75**, 49 (2003).
[37]B. Matthews, R. Fenna, M. Bolognesi, M. Schmid, and J. Olson, J. Mol. Biol. **131**, 259 (1979).
[38]D. E. Tronrud, M. F. Schmid, and B. W. Matthews, J. Mol. Biol. **188**, 443 (1986).
[39]T. M. Wahlund, C. R. Woese, R. W. Castenholz, and M. T. Madigan, Arch. Microbiol. **156**, 81 (1991).
[40]A. Ben-Shem, F. Frolow, and N. Nelson, FEBS Lett. **564**, 274 (2004).
[41]L. G. D. E. Tronrun, J. Wen, and R. E. Blankenship, Photosynth. Res. **100**, 79 (2009).
[42]M. Busch, F. Müh, M. E. Madjet, and T. Renger, J. Phys. Chem. Lett. **2**, 93 (2011).
[43]C. R. Larson, C. O. Seng, L. Lauman, H. J. Matthies, J. Wen, R. E. Blankenship, and J. P. Allen, Photosynth. Res. **107**, 139 (2011).
[44]J. Adolphs, F. Müh, and M. E. Madjet, Photosynth. Res. **95**, 197 (2008).
[45]M. K. Sener, S. Park, D. Lu, A. Damjanovic, T. Ritz, P. Fromme, and K. Schulten, J. Chem. Phys. **120**, 11183 (2004).
[46]See supplementary material at http://dx.doi.org/10.1063/1.4930110 for Hamiltonian parameters and further calculation results relating to influence of network perturbations.
[47]H. Haken and G. Strobl, Z. Phys. **262**, 135 (1973).
[48]A. Eisfield and J. S. Briggs, Phy. Rev. E **85**, 046118 (2012).
[49]G. Tao and W. H. Miller, J. Phys. Chem. Lett. **1**, 891 (2010).
[50]W. H. Miller, J. Phys. Chem. A **105**, 2942 (2001).
[51]G. S. Orf, D. M. Niedzwiedzki, and R. E. Blankenship, J. Phys. Chem. B **118**, 2058 (2014).
[52]W. H. Press, S. A. Teukolsky, W. T. Vetterling, and B. P. Flannery, *Numerical Recipes in Fortran 77: The Art of Scientific Computing* (Cambridge University Press, Cambridge, UK, 1992).
[53]R. Albert, H. Jeong, and A.-L. Barabási, Nature **406**, 378 (2000).
[54]M. E. J. Newman, SIAM Rev. **45**, 167 (2003).
[55]N. Skochdopole and D. A. Mazziotti, J. Phys. Chem. Lett. **2**, 2989 (2011).
[56]K. M. Gaab and C. J. Bardeen, J. Chem. Phys. **121**, 7813 (2004).
[57]R. W. Floyd, Commun. ACM **5**, 345 (1962).
[58]S. Warshall, J. ACM **9**, 11 (1962).